East African Journal of Science, Technology and Innovation, Vol. 6 (Special issue 1): December 2024

Enhanced coconut shell-based activated carbon for water desalination using an adsorption-capacitive deionization hybrid system

[1*]*DAUDI L M.*, [2]*BAIRO A M.*, [2]*OMARI S.*, [2]*ELISADIKI J.*, [2]*MTABAZI G S.*, [2]*SAIDI A V*

[1]Department of Physics, College of Natural and Mathematical Sciences, University of Dodoma P.O B.O.X 338, Dodoma-Tanzania.
[2]Department of Chemistry, College of Natural and Mathematical Sciences, University of Dodoma P.O B.O.X 338, Dodoma-Tanzania.

***Corresponding Author**: liliandaudi98@gmail.com

Abstract

Freshwater scarcity is a global issue, and most water purification technologies are energy-intensive, making them unaffordable for low-income societies. Adsorption-capacitive deionization (ACDI) offers a low-energy solution, making it a potential solution for these societies. This study utilized coconut shells to prepare pristine activated carbon (PAC) electrodes for ACDI by KOH activation at temperatures 700 and 800 ˚C. To enhance the performance of coconut shell-activated carbon electrodes, Tetramethylammonium bromide ((CH3)4N+ Br-) which is a cationic surfactant was used to create positive charges on the surface of PAC to make enhanced activated carbon (EAC) for an ACDI hybrid system application. The surface functional groups were identified by using Fourier Transform Infrared Spectroscopy (FTIR) and pore size distribution and surface area (SA) were identified by the Barret-Joyner-Halenda (BJH) and Brunauer-Emmett-Teller (BET) method under N2 adsorption/desorption isotherm respectively. The PAC and EAC attained maximum specific SA of 175.03 and 751.43 m2/g respectively. The electrochemical properties of PAC electrodes such as specific capacitance (SC) and electrical conductivity were examined using cyclic voltammetry (CV) and electrochemical impedance spectroscopy (EIS) in 6 M of KOH electrolyte using a CS 350 electrochemical cell. The SC of PAC from activated carbon was 376.29 F/g while EAC increased to 628.20 F/g. The salt adsorption capacity of PAC and EAC were 2.78 and 10.96 mg/g respectively. It can be seen that enhancing the AC led to the improvement of specific SA, SC, and salt removal capacity of AC during the desalination experiment.

Keywords: *Adsorption-capacitive deionization; Coconut shell; Enhanced activated carbon; Hybrid system; Pristine activated carbon; Salt removal*

Received: 18/06/24
Accepted: 05/12/24
Published: 20/12/24

Cite as, Daudi *et al., (2024)*. Enhanced coconut shell-based activated carbon for water desalination using an adsorption-capacitive deionization hybrid system. *East African Journal of Science, Technology and Innovation 6 (Special issue 1).*

Introduction

Inadequate fresh water is now a major problem on a global scale. Fresh water is essential for human consumption, domestic uses, and industrial activities (Liu *et al*., 2017). The amount of fresh water available is only 3% of all water available on the Earth while the remaining is saline (Choi *et al*., 2024). Therefore, the desalination process is being used worldwide to

provide people with fresh water. Different advanced technologies such as reverse osmosis, electro-dialysis, filtration, distillation, and clay vessel filtration have been developed to tackle the problem of freshwater shortage (Volfkovich, 2020). Reverse osmosis is a highly extensively utilized method since it removes all disease-causing organisms and the majority of chemical contaminants (Pan *et al*., 2020). It is also a technology that is safe, however, the reverse osmosis process wastes more water, requires expensive maintenance, uses a huge amount of energy to purify one liter of water, eliminates beneficial minerals from the water, and lowers pH (Henthorne & Boysen, 2015). Therefore, alternative technologies that may overcome these challenges are highly needed.

Capacitive deionization (CDI) is a viable water purification process that removes salt ions *from* water using the potential difference between two electrodes (Barcelos, 2021; Qian *et al*., 2023; Sufiani et *al*., 2023). This method is more efficient, with low energy consumption, scalable, easy to operate, environmentally friendly, and cost-effective (Faisal *et al*., 2023). The performance of CDI relies on the resources used in developing its electrodes. Mesoporous carbon, carbon aerogels, carbon black, activated carbon (AC), biochar, metal-coated carbon, composite material, intercalation material, and battery flow electrode materials are mostly used as electrode materials (Qian *et al*., 2023).

Among the stated materials, AC is the commonly frequently utilized for CDI electrodes because of its advanced internal pore structure, high surface area, strong electrical properties, and reduced cost (Choi *et al*., 2024). AC can be generated from carbonaceous source such as coal, wood, animal dung, farm wastes, or biomass, which are plentiful and renewable (Barcelos, 2021). However, the sustainability of some carbon precursors' is making biomass wastes the best choice for most researchers. Materials such as coconut shells (Yeh *et al*., 2015), coffee husks (Puari & Yanti, 2022), banana pills (Taddele, 2017), cabbage leaves (Wang *et al*., 2016), jackfruit peels (Elisadiki, 2020), and peanut shells *(*Zhan *et al*., 2021) have been considered as most suitable precursors for AC preparation due to their lignocellulosic properties, easy availability, and low cost. Also, industrial wastes like waste sludge (Khalili *et al*., 2017) and leather waste (Kong *et al*., 2013) have been used for AC preparation.

However, the performance of AC can be hampered by several factors foristance, lack of selectivity towards specific ion removal, high electrical transfer resistance, poor wettability, an inappropriate pore size distribution, low electrical conductivity, and poor inter-pore connectivity that makes it difficult for ions to diffuse and co-ions to expel (Chen *et al*., 2022). These characteristics can be enhanced using different chemicals for effective CDI and energy reduction. Different chemicals such as nitric acid (HNO_3), sulphuric acid (H_2SO_4), phosphoric acid (H_3PO_4), zinc chloride ($ZnCl_2$), and sodium hydroxide (NaOH) have been used to enhance AC surface (Bhatnagar *et al*., 2013; Guo et al., 2019). Some of the chemicals enhance porosity while others introduce functional groups such as carbonyl, phenols, quinones, lactones, and carboxyl which are important in adsorption (Faisal *et al*., 2023). For example, Demiral et al. (2021), enhanced AC with citric acid to improve copper adsorption from an aqueous solution. The scientists discovered that the surface alteration lowered the specific SA area by 34% and the carbon's point of zero charge (pH) by 0.5 units. Citric acid modification increased adsorption capacity to 14.92 mg/g which was 140% higher than the unmodified one.

Additionally, AC is negatively charged in an aqueous solution, which significantly reduces the scope of its applicability in removing anionic pollutants like ClO_4^-, Cl^- and F^- (Sufiani *et al*., 2019; Zhan *et al*., 2021). Therefore, in this study, Tetramethylammonium bromide (TMAB) whose chemical formula is ($(CH_3)_4N^+Br^-$) was used to create positive charges on the surface of AC. This technique offers a reasonably simple method to introduce positive surface charges on AC since TMAB is a salt of cationic surfactant with a hydrophobic chain that permanently adsorbs on the AC (Shishov *et al*., 2022). Therefore, this study utilized TMAB to enhance the properties of activated carbon derived from coconut shells. Coconut shells were used due to their exceptional chemical and physical features such as high

strength and modulus properties, high abrasion resistance, and easy availability (Zhan *et al*., 2021). To further improve the performance of a hybrid CDI system, cycles of adsorption were run before connecting the electrodes to the potential.This operation is an innovation that incorporates a combination of adsorption (removal of ions from the solution without potential) and CDI (electrosorption of ions owing to potential), and we now refer to it as an adsorption-capacitive deionization (ACDI) hybrid system

Materials and Methods

Materials

Coconut shells used to prepare activated carbon were collected from Sabasaba market –Dodoma-Tanzania. The chemicals employed in this work were of analytical quality and utilized without refinement, including potassium hydroxide (KOH), Tetramethylammonium bromide ($(CH_3)_4N^+Br^-$), hydrochloric acid (HCl), sodium chloride (NaCl), carbon black, ethanol, and polytetrafluoroethylene binder (PTFE).

Activated Carbon Preparation

The shells of coconuts were chopped into small pieces and cleaned in deionized water, dried in sunlight, and grounded to obtain a 1 mm particle size sample. Then carbonized at a temperature of 500 ˚C in a horizontal tube furnace (EQ-OTF-1200 series), and mixed with KOH pellets in a mass ratio of (carbon/KOH) 1:1 and 1:2 at 700 and 800 ˚C for the activation. Consequently, the activated samples were combined with 1M of HCl and stirred to remove inorganic constituents,there after washed with warm distilled water to remove chloride ions (Köseoğlu and Akmil-Başar, 2015). The samples were dried in an oven at 105 ˚Cfor 15 hours and then placed in a desiccator to cool. The samples were then labeled as PAC and stored for enhancement.

Enhancement of AC

In this study, 0.5 wt. % of TMAB was mixed with 2 g of PAC. The obtained solution was shaken in an orbital shaker at a rate of 250 rpm for 3 hours at room temperature. Then filtered, and the solid produced was washed with distilled water until it reached neutral pH, and dried in an oven at 65 ˚C for 15 hours. Then resulted sample was labeled as EAC and stored in the container for further investigation and application.

Characterization

PAC and EAC sample's functional groups were identified with Fourier Transform Infrared Spectroscopy (ATR-FTIR) Pekin Elmer UATR TWO instrument. The specific SA and pore size distribution of PAC and EAC were determined from N_2 adsorption/desorption isotherms using the Brunauer-Emmett-Teller (BET) and Barret-Joyner Halenda (BJH) methods.

Electrochemical Properties Analysis

This was conducted using a CS series 350 electrochemical workstation instrument in a three-electrode cell system. A working electrode was prepared by pressing 80-weight % coconut shell AC, 10-weight % carbon black, and 10-weight % polytetrafluoroethylene binder on a 1cmx1cm piece of nickel foam. Hg/HgO was used as the reference electrode and platinum wire was used as a counter electrode. All electrochemical properties were measured in 6 M of KOH solution at room temperature. Cyclic voltammetry (CV) was carried out at a potential range of -1.0 to 0 V using equation (1) to evaluate the specific capacitance of PAC and EAC. Electrochemical impedance spectra to evaluate the conductivity of PAC and EAC were measured at a range of 1000 Hz to 0.001 Hz.

$$C_v = \frac{\int Idv}{2\gamma m \Delta v} \quad \ldots\ldots\ldots\ldots\ldots\ldots \quad (1)$$

Where C_v is the specific capacitance in F/g, Idv is the integrated area under the CV curve, Δv is the potential window, m is the mass of active material in g, and γ is the potential scan rate in mV/s.

Preparation of CDI electrode

A CDI electrode was made by combining activated carbon, carbon black, and PTFE binder in the ratio 1600:200:200 mg. The mixture was stirred with 15 ml of 99.9% ethanol at 100 ˚C for 30 minutes until paste slurry was formed. A 4 cm x 4 cm electrode was cut and dehydrated in an oven at 60 ˚C for 12h, then cooled to room temperature.

Adsorption-Capacitive Deionization (ACDI) Experiment

This was performed in a batch mode process using both PAC and EAC. The experimental setup included a CDI cell, two water reservoirs, a power supply, a peristaltic pump, and a conductivity meter. A pair of electrodes (4 cm x 4 cm) were put on the current collectors of titanium sheets in the CDI cell. In the first stage, experiments were done without potential application where, 30 ml of feed solution with concentrations of 50, 100, 200, and 500 mg/L were delivered to the CDI via peristaltic pump. The solution circulated and returned to the feed tank at a speed of 10 rpm with a flow rate of 15 ml/min. Then conductivity meter (Hanna instrument (HI) 98129) records the conductivity change and pH in the reservoir. A 1.2 V was supplied using the CS series 350 electrochemical workstation instruments. The salt removal efficiency (Se) and salt adsorption capacity (Γ) were calculated using equations 2 and 3 respectively.

$$Se = \frac{Ci-Cf}{Ci} \times 100\ \% \quad \text{..... (2)}$$

Where *Ci* and *Cf* are the initial and final concentration of solutions after time t respectively in mg/L.

$$\Gamma = \frac{(C_i-C_f)V}{M_e} \quad \text{.....(3)}$$

Where Γ is the electrosorption capacity in mg g^{-}, $C_f$and C_i are the final and initial concentration in mg/L, V is the volume in liter and Me is the total mass of active material in both electrodes in g.

Results

Surface Analysis

Figures 1

(a) and (b) show the nitrogen sorption isotherms and Figures 1 (c) and (d) show BJH pore size distribution ***plots of*** *PAC and EAC at a temperature of 700 ˚C 1:2 and 800 ˚C 1:2 to evaluate porosity.*

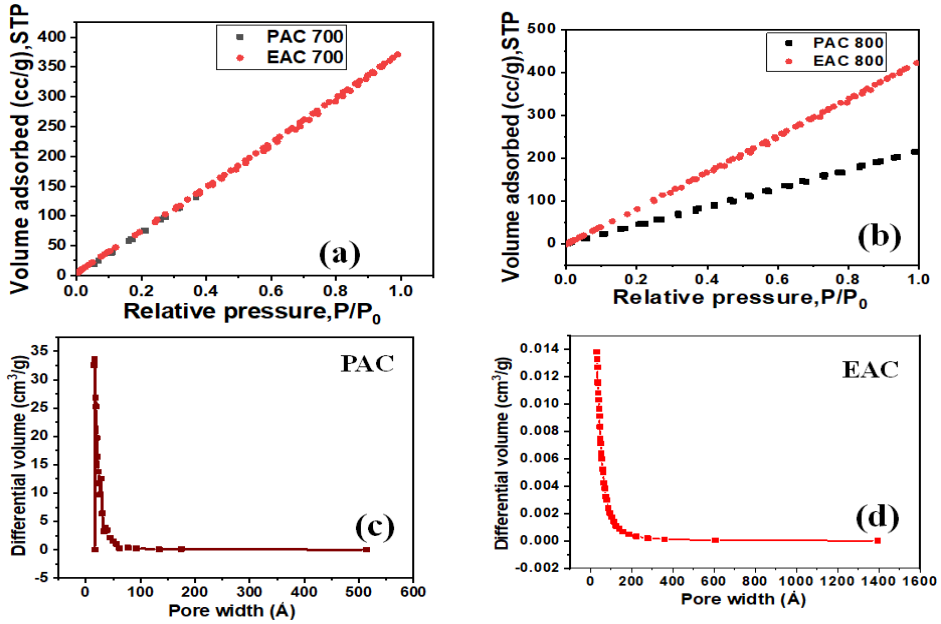

Table 1

BET SA, pore volume, and radius of PAC and EAC at a temperature of 700 ˚C 1:2 and 800 ˚C 1:2.

Parameter	PAC 700	PAC 800	EAC 700	EAC 800
BET SA (m²/g)	171.89	175.03	745.45	751.43
Pore volume(cc/g)	0.359	0.37	0.53	0.59
Pore radius (Å)	10.03	10.05	10.43	11.18

Functional Group Analysis

Figure 2

FTIR spectra in the structures of PAC and EAC at a temperature of 800 ˚C 1:2 from coconut shells.

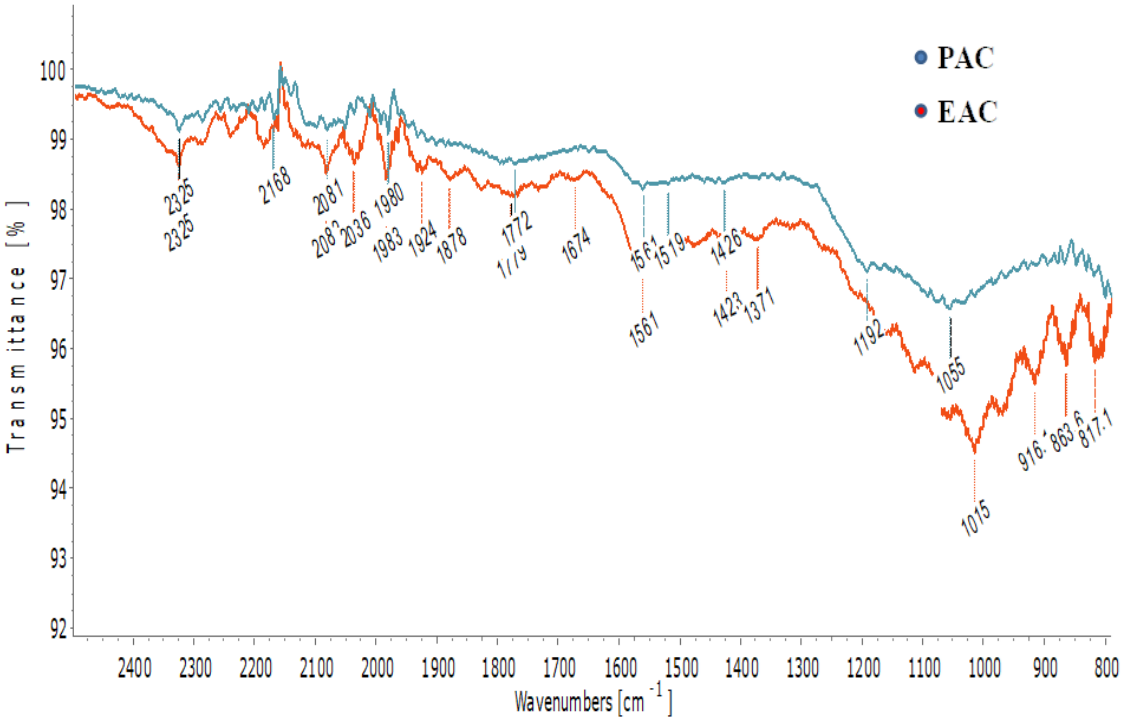

Electrochemical Properties Analysis

CV to obtain SC of both PAC and EAC at a temperature of 700 and 800 ˚C and the CV curves are present in Figure 3 (a), (b), (c), and (d).

The comparison of the SC of PAC and EAC at a temperature of 700 and 800 ˚C at different scan rates was shown in Figure 4 (a) and (b). The electrical conductivity of both PAC and EAC electrodes was examined using an EIS analysis and presented with Nyquist plots in Figure 4 (c) and (d).

Figure 1

Cyclic voltammograms of (a) PAC 700 ˚C 1:2 (b) EAC 700 ˚C 1:2 (c) PAC 800 ˚C 1:2 (d) EAC 800 ˚C 1:2 at different scan rates.

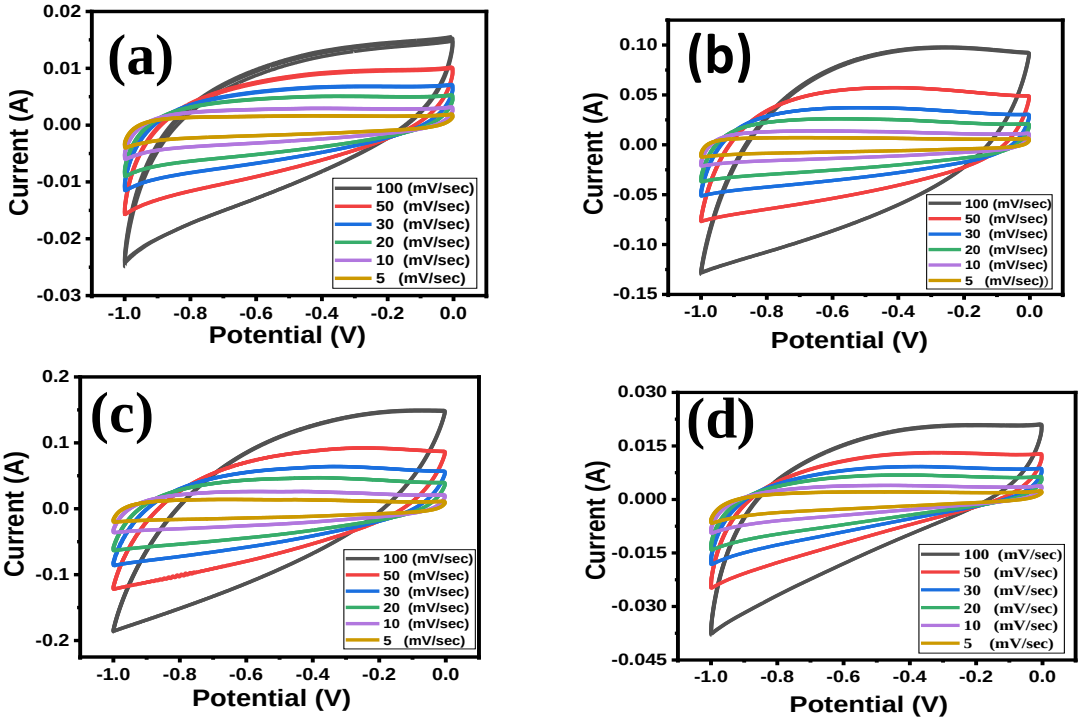

Adsorption-Capacitive Deionization Experiment

The results of conductivity against time for physical adsorption and electrosorption processes to represent hybrid CDI were recorded as shown in Figure 5 (a), (b), (c), and (d). Figures 5 (e) and (f) show the variation of initial concentration on the salt adsorption capacity of PAC and EAC electrodes and the change in pH during the adsorption phase respectively.

By inserting [Figure 5 (a), (b), (c), (d), (e), and (f) here]

The results for the comparison of the adsorption capacity of PAC and EAC at a temperature of 800 ˚C 1:2 are presented in Table 2.

Figure 2

Comparison of specific capacitance for (a) different EAC samples (b) PAC samples at different scan rates, and Nyquist plots of (c) PAC 800 ˚C 1:2 and PAC 700 ˚C 1:2 (d) EAC 800 ˚C 1:2 and EAC 700 ˚C 1:2

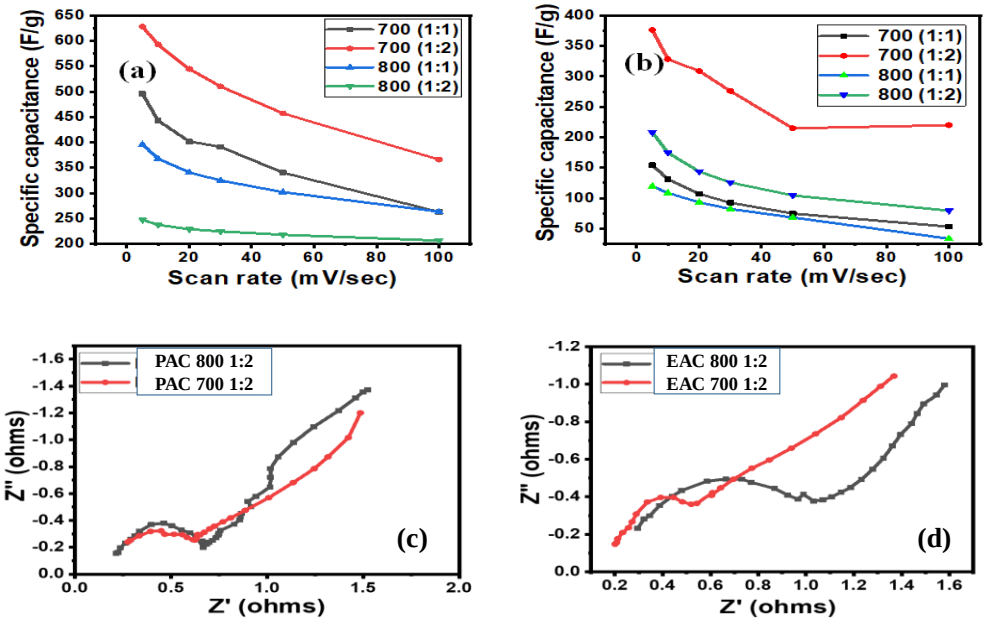

Figure 3

(a), (b), (c) and (d) Relationship between conductivity and time during adsorption-capacitive deionization process for 2 hours at a concentration of 50 and 500 mg/L of both PAC and EAC (d) variation of initial concentration on the salt adsorption capacity of PAC and EAC (f) change in pH with time during adsorption phase at a temperature of 800 ˚C 1:2.

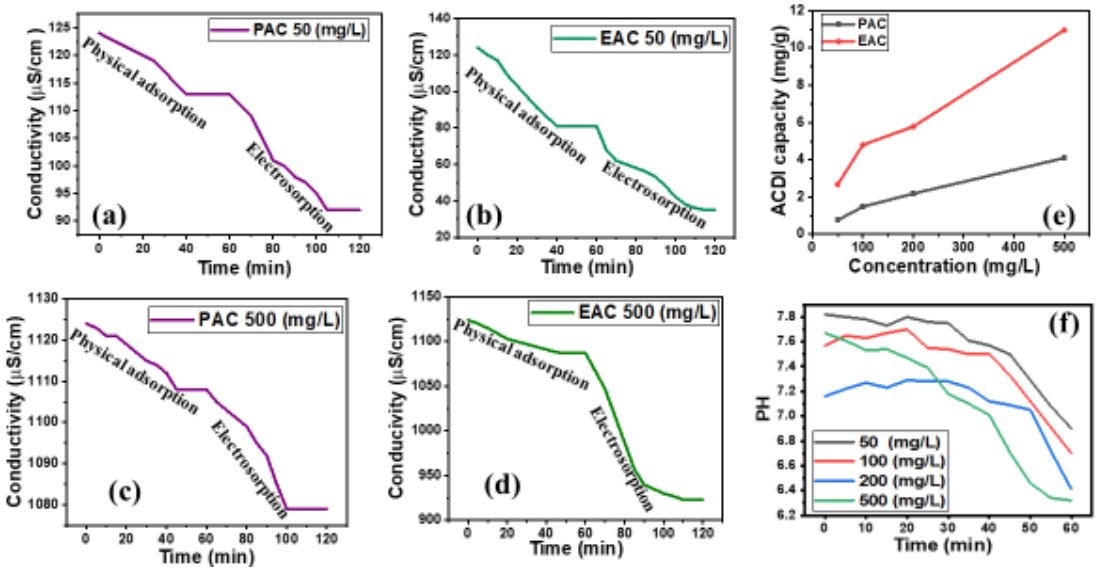

Table 1

alt removal efficiency and the salt adsorption capacity for desalination of NaCl solution with different concentrations at a temperature of 800 ˚C 1:2

Concentration (mg/L)	Salt removal efficiency (%)		Total salt adsorption capacity (mg/g)	
	PAC	EAC	PAC	EAC
500	0.09	17.88	2.78	10.96
200	12.44	25.85	2.18	5.78
100	6.96	24.38	1.48	4.80
50	21.77	72.58	0.76	2.67

Discussion

Surface Analysis

Figures1 (a) and (b) show that activated carbon made from coconut shells exhibits a typical Type I isotherm with a well-defined plateau pointing to microporous structures(Das *et al*., 2015). The rapid vertical rise near $P/P_0 = 1$ indicates bulk condensation of the gas (Achaw & Afrane, 2008). Thus PAC 700, PAC 800, EAC 700, and EAC 800 were termed as microporous. Pore size distribution (Figures 1 (c) and (d)), pore volume, BET SA, and pore radius (Table 1) support this. IUPAC divides pores into three types: micropores (less than 2 nm), mesopores (2-50 nm), and macropores (more than 50 nm) (Dolas et *al*., 2011; Wang *et al*., 2016). In general, it can be said that over 90% of prepared AC consists of micropores. In addition, the nitrogen adsorption/desorption curves of PAC and EAC show that the gradient of the isotherm curve rose dramatically as a result of the process of activation, showing the formation of porous structures after KOH activation. During KOH activation, carbon atoms are burned off and generate CO and CO_2 gases, improving the pore structure of the carbon fibers (Sufiani *et al*., 2019). From Figure 1 (a) and (b) it was observed that as the activation temperature increases to 800 ˚C differential volumes also increase indicating that the materials developed more pores. All samples show that most of the pores are less than 500 Å for PAC and 1400 Å for EAC. As discussed above the presence of micropores in the sample contributes to large SA resulting in improved adsorption performance as confirmed in previous studies by (Qian *et al*., 2023). From Figure 1 (a) and (b) adsorbed volume increased from 0 to 125 cc/g for PAC-700 and from 0 to 180 cc/g for PAC-800 while for EAC-700 it increased from 0 to 375 cc/g and for EAC-800 from 0 to 410 cc/g revealing the enhanced pore size distribution.

From Table 1, PAC-700 before enhancement exhibits a BET SA of 171.89 m^2/g and after enhancement, it increases to 745.45 m^2/g indicating enhanced SA. For PAC-800 before enhancement exhibits a BET SA of 175.03 m^2/g and after enhancement it increases to 751.43 m^2/g, indicating enhanced SA.

Moreover, as indicated in Table 1, the results show that activation temperature has a great impact on BET SA whereby, as the activation temperature increases also BET SA increases. Foristance PAC-700-171.89 m^2/g, PAC-800-175.03 m^2/g, and EAC-700-745.45 m^2/g, EAC-800-751.43 m^2/g, these results prove that as the activation temperature goes high materials are forced to open up and have more microscopic pores, as a result of the discharge of volatile substances that lead to the increase in BET SA of the materials (Sufiani *et al*., 2019). On the other hand, the impact of activation temperature on the pore volume of PAC and EAC was investigated. The results indicate that pore volume increases with the increase in the activation temperature. The main reason for the occurrence of this is that as the temperature increases, it forces the pores of the materials to open up and broaden the

presence hence pore volume increases (Sarkar *et al*., 2020). Furthermore, the influence of pore radius on the activation temperature was investigated, the results obtained show that as the activation temperature increases also pore radius increases, this is caused by the effect of activation temperature on the pore volume of AC materials, because as the volume of a certain pore increases, its radius must also increase because the pore becomes broadening.

Functional Group Analysis

Commonly agricultural residues often contain functional groups like carboxyl, phenol, quinones, and lactones, which can bind pollutants to a certain degree (Sufiani *et al*., 2023). These surface functional groups have an impact on the resulting carbonaceous materials' porous features and adsorption traits (Qian *et al*., 2023). Similar effects are seen in the surface charges of carbonaceous materials in water-based solutions when these groups are created(Elisadiki & King'ondu, 2020). From Figure 2, it was observed that there is some difference in peaks recorded from PAC and EAC. A peak at 2325 cm^{-1} corresponds to a carboxylic acid with a stretching vibration of C=O (Demiral *et al*., 2021). A band with 2051 cm^{-1} was due to the C=N stretching mode of nitriles (Demiral *et al*., 2021). The band at 1980 cm^{-1} can be allocated to the CH_2≡CH2- extending mode of alkynes (Danish *et al*., 2013). A band at 1192 cm^{-1} related to the C-C bonds of alkane groups (Yang *et al*., 2015). A band with 1560 cm^{-1} and 1561 cm^{-1} can be assigned to $-CH_2$ and CH_2 twisting modes of alkenes (Elena & Miri, 2018). Moreover, a band at 1388 cm^{-1} was due to alkanes' C-H twisting (CH_2 and CH_2) mode (Das *et al*., 2015). A band at 1051 cm^{-1} can be assigned to the C-O bending mode of alcohol, ether, and carboxylic acid (IkhtiarBakti and Gareso, 2018). A band at 1789 cm^{-1} can be assigned to the C=O carboxyl group of acetyl groups (Sujiono *et al*., 2022). The use of TMAB chemical leads to the creation of new functional groups as illustrated in EAC spectra for instance, considering the band of salt at 1371 cm^{-1} due to uneven angular twisting of methyl groups of quaternary ammonium (Elena and Miri, 2018). A band at 916 cm^{-1} corresponded to the O-H of carboxylic acid. The band at 817 cm^{-1} is related to the C-H bending of aromatic groups. A band of 1015 cm^{-1}, which corresponded to ($C-N^+$) bands was not detected in the infrared spectrum corresponding to PAC. Hence this proves that enhancement was conducted. Also from this study, some functional groups such as O-H did not appear on PAC this is because, during the activation process, most of the functional adsorption peaks are lost as volatile matter when heat is supplied to the sample (Taddele, 2017). This evidences that the activation process has been effectively accomplished and the carbon retains some functional groups.

Electrochemical Properties Analysis

From Figure 3, it was observed that all CV curves exhibit almost similar shapes and no oxidation-reduction peaks were observed. The consistency in CV curve forms at most scan rates (SR) may imply that the same or comparable electrolytic processes occur in the cell regardless of the SR used; this suggests improved charge transfer stability of the device (Sujiono *et al*., 2022). Furthermore, all curves have an approximately similar shape indicating good charge storage and capacitive capability (Elisadiki, 2020).From Figure 4 it can be seen that at SR of 5 mV/s, PAC 700 1:1 and PAC 700 1:2 attained a SC of 154.20 F/g and 376.29 F/g respectively, while PAC 800 1:1and EAC 800 1:2 exhibited low SC of 119.40 F/g and 207.89 F/g respectively. Moreover, the SC for EAC 800 1:1, EAC 800 1:2 EAC 700 1:1, and EAC 700 1:2 were 395.72, 247.15, 495.97, and 628.20 F/g respectively. Also, at a SR of 100 mV/s, the value of SC for both PAC and EAC decreased whereby, PAC 700 1:1 exhibited a SC of 53.11 F/g, while PAC 700 1:2 exhibited SC of 219.94 F/g. Furthermore, PAC 800 1:1 attained SC of 33.42 F/g, while PAC 800 1:2 attained SC of 79. 42 F/g.

From the results, it can be observed that SC of both PAC and EAC increases with a decrease in SR as shown in Figure 4 (a) and (b) for the reason that, at a low SR the electrolyte has more time to contact the electrode pores and more ions are adsorbed leading to high SC. Also, this may be attributed to the increase in several charges during enhancement. The ratio of C/KOH used during the activation process affected the SC of AC, as the amount of KOH increases, it means that KOH and carbon are in full contact, so the

activation degree is improved and the pore tends to develop leading to high SA hence SC increases (Puari and Yanti, 2022). From the results of Figure 4 (a) and (b) as the activation temperature increases, SC drops, the electrical resistance of AC is lowered, and the transfer of charge becomes easier, which may be validated by an EIS analysis. Figure 4 (c) and (d) (Elisadiki, 2020). The improvement in SC of EAC is due to richer porosity and the higher specific surface area developed by activation temperature. Theoretically, the SC of the carbon electrodes increases with the increase in the SA of carbon (Yeh *et al*., 2015) which agrees with our results, whereby EAC exhibits the largest BET SA and SC. Moreover, it is observed that closed areas under the CV curves of EAC are large, indicating its high capacitive performance. As a result, EAC exhibits high SC.

In comparing the results of the specific capacitance of coconut shell AC used in this study from former biomass materials used in the other studies, the comparison was done by considering the specific capacitance obtained at a SR of 10 mV/s as seen in Table 3. It can be demonstrated that enhanced AC prepared from coconut shells achieved a greater SC compared to others. The greater SC was due to polarization on the AC surface, high specific SA, and pore volume of AC which resulted from the physical function of the TMAB functional groups.

Table 2

Comparison of specific capacitance of coconut shells AC from another biomass material at a scan rate of 10 mV/s.

Biomass materials	Activating agent	Activation temperature (˚C)	Scan rate (mV/s)	Specific capacitance (F/g)	References
Cotton stalk	H_3PO_4	750	10	283	(Li *et al*., 2017)
Coffee husks	H_3PO_4	800	10	110	(Duan *et al*., 2017)
Watermelon	H_3PO_4	900	10	425	(Rambabu *et al*., 2020)
Mushrooms	NaOH	800	10	228	(Shi *et al*., 2022)
Jackfruit peels	KOH and H_3PO_4	700	10	198	(Elisadiki *et al*., 2019)
Coconut shell	KOH	700	10	592.93	This study

The electrical conductivity of EAC electrodes was examined using an EIS analysis and presented with Nyquist plots in Figure 4 (c) and (d). From the Figure Nyquist plots consist of a semi-circle area recorded at high frequency and the non-vertical region observed at low frequency makes up the major two regions for both electrodes. The semi-circle area at high frequency corresponds to the charge transfer resistance at the electrode/electrolyte contact (Xing *et al*., 2023). In addition, a two-layer capacitor corresponded to the slope of the tail (non-vertical zone). The diameter of the semi-circle corresponded to the charge-transfer resistance of the electrodes and the solution interface (Hidayu and Muda, 2016). It was detected that the diameter of the semicircle increases with the increase in temperature signifying that at high-temperature polarization resistance is high compared to low temperature. The electrodes' equivalent series resistances (ESR) were presented by the intersection of the curves at the real axis in the high-frequency region(Liang *et al*., 2020). The smaller the ESR value, the smaller the internal resistance (charge transfer resistance). ESR values recorded as appeared in Figure 4 (c) and (d) were 0.61, 0.62,

1.1, and 0.58 Ω for PAC 1:2–800, PAC 1:2-700, EAC 1:2–800, and EAC 1:2–700 respectively. These values show that the produced carbon possesses small internal resistance and better electrical conductivity.

Adsorption-Capacitive Deionization Experiment

Because of their high specific SA, strong electrical conductivity, and large average pore volume, the PAC 800 1:2 and EAC 800 1:2 electrodes were chosen to study CDI desalination performance. This experiment involved physical adsorption and electrosorption (hybrid CDI system). In Figure 5 (a), (b), (c), and (d) for both PAC and EAC the NaCl solution's conductivity decreased as the time increased during the physical and electrosorption processes. This implies that ions were adsorbed. During the experiment, it was observed that EAC exhibits the highest electrosorption capacity than PAC. EAC's better performance might be due to higher BET surface area, pore radius, and total pore volume, as shown in Table 1, as well as good electrochemical properties(Liang *et al*., 2020).

From the results, the salt adsorption capacity of PAC at a concentration of 50, 100, 200, and 500 mg/L were 0.36, 0.61, 0.78, and 0.87 mg/g respectively during physical adsorption. And 0.42, 0.87, 1.40, and 2.02 mg/g during electrosorption. These results show that during the electrosorption stage, more ions were adsorbed compared to the physical sorption stage. EAC during physical adsorption exhibited salt adsorption capacity of 0.87, 0.98, 1.67, and 2.40 mg/g at a concentration of 50, 100, 200, and 500 mg/L respectively. And during the electrosorption process the salt adsorption capacity were 1.80, 3.82, 4.11, and 8.56 mg/g indicating that during the electrosorption process, more ions were adsorbed. These whole results indicate that salt ions were removed by both physical adsorption and electrosorption bringing in the concept of an adsorption-capacitive deionization hybrid system. However, in an ACDI hybrid system high adsorption capacity is much more pronounced during the electrosorption phase.

The results obtained indicate that ACDI capacity increases with the increase in concentration of feed solution as indicated in Table 2. In previous studies, it was reported that the ion's adsorption capacity on the surface of the electrode increases as the concentration increases. Due to the reason that when the concentration increases the solution resistance decreases resulting in an increased concentration gradient and the EDL formation becomes easier (Choi *et al*., 2024). The pH of the solution was monitored along the electrosorption process to study whether oxidation was taking place on the electrode surface (Figure 5(f)). It can be seen that there was a slight change in the pH of the solution probably due to the oxidation of carbon, anode, water, and chloride ions. This resulted in a fall in H^+ concentration, which may cause the measured conductivity value to not accurately represent solution ionic strength. As a result, it is impossible to determine whether the conductivity recorded was purely due to Na^+ and Cl^- ions, or whether H^+ ions also influenced the final conductivity observed.

Conclusion

In this study, AC was prepared from high carbon content, low ash, inexpensive available, and environmentally friendly coconut shell biomass materials through chemical activation methods at 700 and 800 ˚C with varied ratios of carbon and KOH. The properties of AC were enhanced by simply using quaternary ammonium salt (Tetramethylammonium bromide). The temperature and chemicals used during the activation have great impacts on the electrochemical properties, textural properties, and desalination performance of synthesized AC electrodes. Electrochemical performance analysis revealed that EAC electrodes exhibited the highest specific capacitance compared to PAC electrodes, indicating that EAC has a high electrosorption capacity foristance considering a SR of 5 Mv/s EAC 800 1:1 has a great SC of 395.72 F/g compared to PAC which has 119.40 F/g.

Also from the ACDI experiment the salt adsorption capacities of EAC electrode at different concentrations of 500, 200, 100, and 50mg/L were 10.96, 5.78, 4.80, and 2.67 mg/g respectively. As compared to other literature EAC has shown effective removal of Na^+ and Cl^- ions from NaCl solution. Salt removal is mainly caused by the ion's electrostatic attraction on the

surface of a charged electrode as a result of EDL creation. As a result of its high BET SA and total pore volume, EAC formed from coconut shells can be regarded as a suitable material for manufacturing CDI electrodes for water desalination applications. The use of an ACDI hybrid system improves salt removal capacity and probably minimize energy used during water desalination.

Recommendations

About the findings of this research, some of the proposals are made:

Future studies should focus on increasing the size of the electrode since it performs an essential part inimproving ion removal. With the increase in electrode size, ion sorption increases.

Future study to consider calculating energy for a pure CDI system and compare it with the proposed hybrid CDI system.

Postmotum of pristine and used electrodes to be conducted to get more insight into salt removal mechanism.

Acknowledgment

Authors express their gratitude to The World Academy of Science (TWAS) for providing research equipment and consumables used in this study under grant number 21-315 RG/CHE/AF/AC-G -FR3240319512.

References

Achaw, O.-W., & Afrane, G. (2008). The evolution of the pore structure of coconut shells during the preparation of coconut shell-based activated carbons. *Microporous and mesoporous materials*, *112*(1-3), 284-290.

Barcelos, K. M. (2021). Development of stable and high-performance polyaniline activated carbon electrodes for capacitive deionization desalination.

Bhatnagar, A., Hogland, W., Marques, M., &Sillanpää, M. (2013). An overview of the modification methods of activated carbon for its water treatment applications. *Chemical Engineering Journal*, *219*, 499-511.

Chen, L., He, F., &Li, F. (2022). Denitrification enhancement by electro-adsorption/reduction in capacitive deionization (CDI) and membrane capacitive deionization (MCDI) with copper electrode. *Chemosphere*, *291*, 132732.

Choi, H., Kim, D., Kim, D. G., Kim, Y., Park, J. G., Kim, M.-G., Jung, Y.-G., Yoo, J., Baek, J., &Kang, S. (2024). Improved performance of flow-electrode capacitive mixing through N-doping of activated carbon. *Desalination*, *581*, 117591.

Danish, M., Hashim, R., Ibrahim, M. M., &Sulaiman, O. (2013). Effect of acidic activating agents on surface area and surface functional groups of activated carbons produced from Acacia mangium wood. *Journal of Analytical and Applied Pyrolysis*, *104*, 418-425.

Das, D., Samal, D. P., &Meikap, B. (2015). Preparation of activated carbon from green coconut shell and its characterization. *J. Chem. Eng. Process Technol*, *6*(5), 1-7.

Demiral, İ., Samdan, C., &Demiral, H. (2021). Enrichment of the surface functional groups of activated carbon by modification method. *Surfaces and Interfaces*, *22*, 100873.

Dolas, H., Sahin, O., Saka, C., &Demir, H. (2011). A new method on producing high surface area activated carbon: the effect of salt on the surface area and the pore size distribution of activated carbon prepared from pistachio shell. *Chemical engineering journal*, *166*(1), 191-197.

Duan, X., Srinivasakannan, C., Wang, X., Wang, F., &Liu, X. (2017). Synthesis of activated carbon fibers from cotton by microwave induced H3PO4 activation. *Journal of the Taiwan Institute of Chemical Engineers*, *70*, 374-381. https://doi.org/https://doi.org/10.1016/j.jtice.2016.10.036

Elena, P., &Miri, K. (2018). Formation of contact active antimicrobial surfaces by covalent grafting of quaternary ammonium

compounds. *Colloids and Surfaces B: Biointerfaces*, *169*, 195-205.

Elisadiki, J. (2020). Mesoporous carbon materials derived from artocarpus heterophyllus for water desalination and defluoridation using capacitive deionization.

Elisadiki, J., Jande, Y. A. C., Machunda, R. L., &Kibona, T. E. (2019). Porous carbon derived from Artocarpus heterophyllus peels for capacitive deionization electrodes. *Carbon*, *147*, 582-593.

Elisadiki, J., &King'ondu, C. K. (2020). Performance of ion intercalation materials in capacitive deionization/electrochemical deionization: A review. *Journal of Electroanalytical Chemistry*, *878*, 114588.

Faisal, H. A., Mohammed, A. K., Sbani, N. H. A., & Isaha, W. N. R. W. (2023). Preparation, characterization, and tetracycline adsorption efficiency of Tea residue-derived activated carbon. *Al-Khwarizmi Engineering Journal*, *19*(4), 1-15.

Guo, Q., Liu, Y., &Qi, G. (2019). Application of high-gravity technology NaOH-modified activated carbon in rotating packed bed (RPB) to adsorb toluene. *Journal of Nanoparticle Research*, *21*(8), 1-14.

Henthorne, L., & Boysen, B. (2015). State-of-the-art of reverse osmosis desalination pretreatment. *Desalination*, *356*, 129-139.

Hidayu, A., & Muda, N. (2016). Preparation and characterization of impregnated activated carbon from palm kernel shell and coconut shell for CO2 capture. *Procedia Engineering*, *148*, 106-113.

IkhtiarBakti, A., and Gareso, P. L. (2018). Characterization of active carbon prepared from coconuts shells using FTIR, XRD & SEM techniques. *J. Ilm. Pendidik. Fis. Al-Biruni*, *7*, 33-39.

Khalili, A., Jamshidi, S., Khalesidoust, M., Vesali Naseh, M., Akbarzadeh, A., Mamaghani Nejad, M., Mohebbi, M., &Sameni, F. (2017). Evaluation of sewage sludge for incineration (case study: Arak wastewater treatment plant). *Environmental Energy and Economic Research*, *1*(3), 249-258.

Kong, J., Yue, Q., Wang, B., Huang, L., Gao, B., Wang, Y., &Li, Q. (2013). Preparation and characterization of activated carbon from leather waste microwave-induced pyrophosphoric acid activation. *Journal of analytical and applied pyrolysis*, *104*, 710-713.

Köseoğlu, E.,&Akmil-Başar, C. (2015). Preparation, structural evaluation and adsorptive properties of activated carbon from agricultural waste biomass. *Advanced Powder Technology*, *26*(3), 811-818. https://doi.org/https://doi.org/10.1016/j.apt.2015.02.006

Li, K., Rong, Z., Li, Y., Li, C., &Zheng, Z. (2017). Preparation of nitrogen-doped cotton stalk microporous activated carbon fiber electrodes with different surface area from hexamethylenetetramine-modified cotton stalk for electrochemical degradation of methylene blue. *Results in Physics*, *7*, 656-664. https://doi.org/https://doi.org/10.1016/j.rinp.2017.01.030

Liang, Q., Liu, Y., Chen, M., Ma, L., Yang, B., Li, L., &Liu, Q. (2020). Optimized preparation of activated carbon from coconut shell and municipal sludge. *Materials Chemistry and Physics*, *241*, 122327.

Liu, J., Yang, H., Gosling, S. N., Kummu, M., Flörke, M., Pfister, S., Hanasaki, N., Wada, Y., Zhang, X., &Zheng, C. (2017). Water scarcity assessments in the past, present, and future. *Earth's future*, *5*(6), 545-559.

Pan, S.-Y., Haddad, A. Z., Kumar, A., &Wang, S.-W. (2020). Brackish water desalination using reverse osmosis and capacitive deionization at the water-energy nexus. *Water research*, *183*, 116064.

Puari, A. T., &Yanti, N. R. (2022). Utilisation of Exhausted Coffee Husk as Low-Cost Bio-Sorbent for Adsorption of Pb2+. *Tropical Life Sciences Research*, *33*(3), 229.

Qian, A., Wu, H., Wang, G., Sun, N., Cheng, H., Zhang, K., & Cheng, F. (2023). Freeing Fluoride Termination of Ti3C2T x via Electrochemical Etching for High-Performance Capacitive Deionization.

ACS Applied Materials and Interfaces, *15*(7), 9203-9211.

Rambabu, K., Bharath, G., Hai, A., Luo, S., Liao, K., Haija, M. A., Banat, F., & Naushad, M. (2020). Development of watermelon rind derived activated carbon/manganese ferrite nanocomposite for cleaner desalination by capacitive deionization. *Journal of cleaner production*, *272*, 122626.

Sarkar, S., Arya, A., Gaur, U. K., & Gaur, A. (2020). Investigations on porous carbon derived from sugarcane bagasse as an electrode material for supercapacitors. *Biomass and Bioenergy*, *142*, 105730.

Shi, J., Guo, C., Lei, C., Liu, Y., Hou, X., Zheng, X., & Hu, Q. (2022). High-performance biochar derived from the residue of Chaga mushroom (Inonotus obliquus) for pollutants removal. *Bioresource technology*, *344*, 126268.

Shishov, A., Dubrovsky, I., Kirichenko, S., &Bulatov, A. (2022). Behavior of quaternary ammonium salts and terpenoids-based deep eutectic solvents in aqueous phase. *Journal of Molecular Liquids*, *347*, 117987.

Sufiani, O., Elisadiki, J., Machunda, R. L., &Jande, Y. A. (2019). Modification strategies to enhance electrosorption performance of activated carbon electrodes for capacitive deionization applications. *Journal of Electroanalytical Chemistry*, *848*, 113328.

Sufiani, O., Elisadiki, J., Tanaka, H., Teshima, K., Sahini, M. G., Machunda, R. L., and Jande, Y. A. (2023). Adsorption-capacitive deionization hybrid system with activated carbon of modified potential of zero charge. *Environmental Research*, *219*, 115114.

Sujiono, E. H., Zabrian, D., Zharvan, V., &Humairah, N. (2022). Fabrication and characterization of coconut shell activated carbon using variation chemical activation for wastewater treatment application. *Results in Chemistry*, *4*, 100291.

Taddele, A. (2017). Synthesis, Process Parameters Optimization and Characterization of Banana Peel Based Bio-plastic.

Volfkovich, Y. M. (2020). Capacitive deionization of water (a review). *Russian Journal of Electrochemistry*, *56*(1), 18-51.

Wang, P., Wang, Q., Zhang, G., Jiao, H., Deng, X., &Liu, L. (2016). Promising activated carbons derived from cabbage leaves and their application in high-performance supercapacitors electrodes. *Journal of Solid State Electrochemistry*, *20*, 319-325.

Xing, L.-a., Yang, F., Zhong, X., Liu, Y., Lu, H., Guo, Z., Lv, G., Yang, J., Yuan, A., &Pan, J. (2023). Ultra-microporous cotton fiber-derived activated carbon by a facile one-step chemical activation strategy for efficient CO2 adsorption. *Separation and Purification Technology*, *324*, 124470.

Yang, F., Sun, W., Hu, Y., &Long, S. (2015). Cationic flotation of scheelite from calcite using quaternary ammonium salts as collector: Adsorption behavior and mechanism. *Minerals Engineering*, *81*, 18-28.

Yeh, C.-L., Hsi, H.-C., Li, K.-C., &Hou, C.-H. (2015). Improved performance in capacitive deionization of activated carbon electrodes with a tunable mesopore and micropore ratio. *Desalination*, *367*, 60-68.

Zhan, Y., Zhou, H., Guo, F., Tian, B., Du, S., Dong, Y., &Qian, L. (2021). Preparation of highly porous activated carbons from peanut shells as low-cost electrode materials for supercapacitors. *Journal of Energy Storage*, *34*, 102180.